Nanoscale Res Lett (2010) 5:654–668
DOI 10.1007/s11671-009-9508-2

NANO REVIEW

Carbon Nanotubes for Supercapacitor

Hui Pan · Jianyi Li · Yuan Ping Feng

Received: 7 June 2009 / Accepted: 9 December 2009 / Published online: 5 January 2010

Abstract As an electrical energy storage device, supercapacitor finds attractive applications in consumer electronic products and alternative power source due to its higher energy density, fast discharge/charge time, low level of heating, safety, long-term operation stability, and no disposable parts. This work reviews the recent development of supercapacitor based on carbon nanotubes (CNTs) and their composites. The purpose is to give a comprehensive understanding of the advantages and disadvantages of carbon nanotubes-related supercapacitor materials and to find ways for the improvement in the performance of supercapacitor. We first discussed the effects of physical and chemical properties of pure carbon nanotubes, including size, purity, defect, shape, functionalization, and annealing, on the supercapacitance. The composites, including CNTs/oxide and CNTs/polymer, were further discussed to enhance the supercapacitance and keep the stability of the supercapacitor by optimally engineering the composition, particle size, and coverage.

Keywords Carbon nanotubes · Supercapacitor · Oxide/nanotube composite · Polymer/nanotube composite

H. Pan · Y. P. Feng
Department of Physics, National University of Singapore, Singapore 117542, Singapore

H. Pan (✉)
Institute of High Performance Computing, 1 Fusionopolis Way, Singapore 138632, Singapore
e-mail: panh@ihpc.a-star.edu.sg

J. Li
Institute of Chemical and Engineering Sciences, 1 Pesek Road, Jurong Island, Singapore 627833, Singapore

Introduction

Electrical energy storage is required in many applications demanding local storage or local generation of electric energy. A storage device to be suitable for a particular application must meet all the requirements in terms of energy density (Wh) and maximum power (W) as well as size, weight, initial cost and life, etc. Supercapacitors fill in the gap between batteries and conventional capacitors, covering several orders of magnitude both in energy and in power densities. They are an attractive choice for the energy storage applications in portable or remote apparatuses where batteries and conventional capacitors have to be over-dimensioned due to unfavorable power-to-energy ratio [1, 2]. In electric, hybrid electric, and fuel cell vehicles, supercapacitors will serve as a short-time energy storage device with high power capability and allow storing the energy from regenerative braking. Increasing applications also appear in telecommunications such as cellular phones and personal entertainment instruments.

An ultracapacitor or supercapacitor can be viewed as two nonreactive porous plates, or electrodes, immersed in an electrolyte, with a voltage potential applied across the collectors. A porous dielectric separator between the two electrodes prevents the charge from moving between the two electrodes (Fig. 1). Supercapacitors are generally classified into two types: pseudocapacitor and electric-double-layer capacitor. The electrical charge can be built up in the pseudocapacitor via an electron transfer that produces the changes in chemical or oxidization state in the electroactive materials according to Faraday's laws related to electrode potential, that is, the basis of energy storage in pseudocapacitor is Faradaic charge transfer. The charge process in the electric-double-layer capacitor (EDLC) is non-Faradaic, i.e. ideally no electron transfer takes place

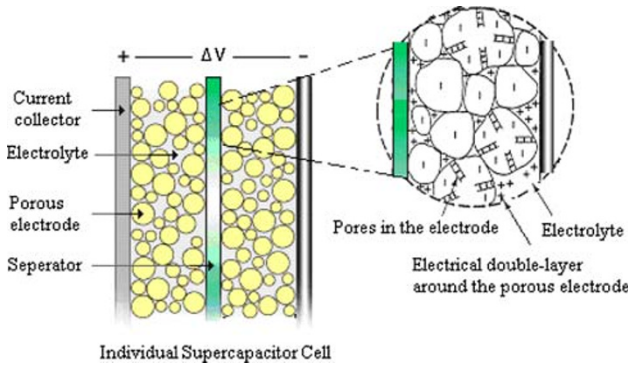

Fig. 1 A presentation of supercapacitor. http://en.wikipedia.org/wiki/Supercapacitor

across the electrode interface and the storage of electric charge and energy is electrostatic [1]. However, the EDLC with various high-area carbon electrodes also exhibit a small but significant pseudocapacitance due to electrochemically active redox functionalities.

The electrical energy (E) accumulated in a supercapacitor is related to the capacitance (C) or the stored charges (Q) and voltage (V) by following formula:

$$E = \frac{CV^2}{2} = \frac{QV}{2}. \quad (1)$$

The capacitance and stored charge depend essentially on the electrode material used, whereas the operating voltage is determined by the stability window of the electrolyte. The use of high-capacitance materials is a key factor for the improvement in the energy density. Generally, the supercapacitor can provide higher power than most batteries, because a large amount of charges (Q) can be stored in the double layers. But, the power density, as indicated in the following formula, is relatively low because of the series resistance.

$$P = \frac{V^2}{4R_S} \quad (2)$$

where R_s represents the equivalent series resistance (ERS) of the two electrodes. The improvement in the power and power density requires the development of materials with high capacitance and low resistance, as indicated in Eqs. 1 and 2.

A variety of materials, including oxide, polymer, carbon and their composites, can be used as the electrodes of supercapacitor. Pseudocapacitor utilizes conducting polymers (such as, polyacetylene, polypyrrole, and polyaniline [3–12]), metal oxides (such as RuO_2 and Co_3O_4 [13–27]), or polymer-oxide composite [26, 28] as electrode materials. The chemical or oxidization state changes in the electrodes induced by the Faradiac charge transfer in the pseudocapactive behavior may affect the cycling stability and limit their application due to high resistance and poor stability, although the specific capacitance of $RuO_2{\cdot}0.5H_2O$ can be as high as 900 F/g [29]. EDLC normally is developed using porous carbon materials (such as activated carbon) as electrode, and the electrical charge is electrostatically accumulated at the electrode/electrolyte interface [30–42]. Carbon aerogel (CA) or other types of carbon materials such as carbon black or carbon cloth are widely used in these supercapacitors. Generally, high surface area in carbon materials is characteristic of highly developed microporous structure, which is however unfavorable for the electrolyte wetting and rapid ionic motions, especially at high current loads. The combination of high surface area carbon aerogel with large specific capacity of oxide or polymer would result in high power and power density, and stability by utilizing both the faradaic capacitance of the metal oxide or polymer and the double-layer capacitance of the carbon [43–46].

Carbon nanotubes (CNTs) have been widely studied since their discovery in 1991 [47] and attracted extensive attention due to their intriguing and potentially useful structural, electrical and mechanical properties. CNTs are formed when a graphite sheet is curled up into cylinders, including single-walled CNT (SWCNT) and multi-walled CNT (MWCNT) [48]. CNTs have a novel structure, a narrow distribution of size in the nanometer range, highly accessible surface area, low resistivity, and high stability [47–52]. These features suggest that CNTs are suitable materials for polarizable electrodes. Both SWCNTs and MWCNTs have been studied for electrochemical supercapacitor electrodes due to their unique properties [53–59]. On the other hand, composites incorporating a nanotubular backbone coated by an active phase with pseudocapacitive properties, such as CNT/oxide composite, represent an important breakthrough for developing a new generation of supercapacitors based on three basic reasons [32, 60–64]: (1) the percolation of the active particles is more efficient with nanotubes than with the traditional carbon materials; (2) the open mesoporous network formed by the entanglement of nanotubes allows the ions to diffuse easily to the active surface of the composite components; and (3) since the nanotubular materials are characterized by a high resiliency, the composite electrodes can easily adapt to the volumetric changes during charge and discharge, which improves drastically the cycling performance. The first two properties are essential to lower the equivalent series resistance (R_s) and consequently increase the power density. In this review, we will focus on recent progress on the CNT-based supercapacitors to investigate the effects of the CNTs and corresponding composites on the performance of the supercapacitors and possible ways for the improvement in the performance. The review is organized into five sections. The brief introduction to the supercapacitor is presented in "Introduction". "Supercapacitor from CNTs" focuses on the pure CNTs-based supercapacitors.

Supercapacitor from CNT/oxide composite is discussed in "Supercapacitor from CNT and oxide composite". Supercapacitor from CNT/polymer composite is investigated in "Supercapacitor from CNT and polymer composite". Finally in "Summary", some concluding remarks are given.

Supercapacitor from CNTs

In 1997, Niu et al. [53] first suggested that CNTs could be used in supercapacitors. The MWCNTs were functionalized in nitric acid with functional groups introduced on the surface. These functionalized MWCNTs had a specific area of 430 m^2/g, a gravimetric capacitance of 102 F/g and an energy density of 0.5 W·h/kg obtained at 1 Hz on a single-cell device, using 38 wt% sulfuric acid as the electrolyte. Although 90% of the catalyst residue was removed, the remaining catalyst in the MWCNTs (mainly within the inner of the tubes) would affect the performance of the supercapacitor. The pseudocapacitance could be induced by the functional groups and the remaining catalyst. Therefore, both of the Faradiac and non-Faradiac processes were involved in the CNTs-based supercapacitor. The redox response observed on the cyclic voltammetric (CV) plot of the SWCNT-based electrodes also indicated that the pseudocapacitance was really occurred to the CNT-based capacitor due to the functional groups and impurities [65]. However, it was demonstrated that the performance of the purified SWCNT, where the catalyst (Fe) was removed by thermal oxidization followed by immersion in HCl, was not as great as expected because of the formation of amorphous carbon by the thermal oxidization [66]. It is difficult to totally remove the catalyst from the catalyst-assisted CNTs and keep the graphitization at the same time, and then the effect of the catalyst is always there. To simplify the discussion, we firstly focus on the structural properties of CNTs, such as diameter, length, and pore size, which play an important role on the EDLC, and discuss the catalyst's and functional groups' effects later.

Effects of Structure

The amount of electrical charge accumulated due to electrostatic attraction in EDLC depends on the area of the electrode/electrolyte interface that can be accessed by the charge carriers. The higher surface area of the electrode material could leads to higher capacitance if the area can be fully accessed by the charge carriers. However, the higher surface area does not always result in higher capacitance because the capacitance also depends on the pore size, the size distribution and conductivity. Higher capacitance can be achieved by optimizing all of the related factors. For example, the vertically aligned CNTs with the diameter of about 25 nm and a specific area of 69.5 m^2/g had a specific capacitance of 14.1 F/g and showed excellent rate capability, which were better than those of entangled CNTs due to the larger pore size, more regular pore structure and more conductive paths [67, 68].

The effects of structures and diameters of CNTs, and microtexture and elemental composition of the materials on the capacitance were systematically investigated by Frackowiak et al. [56]. Table 1 shows the capacitance increases with the increase in the specific surface area. The smallest value is obtained in CNTs with closed tips and graphitized carbon layers, where the mesopore volume for the diffusion of ions and the active surface for the formation of the electrical double layer are very limited in this material. The nanotubes with numerous edge planes, either due to herringbone morphology (A900Co/Si) or due to amorphous carbon coating (A700Co/Si), are the most efficient for the collection of charges. Quite moderate performance is given by straight and rigid nanotubes of large diameter (P800Al) despite a relatively high specific surface area. However, taking into account the diameter of the central canal, it is too large in comparison with the size of the solvated ions. On the other hand, this particular behavior could be also due to a very hydrophobic character of these tubes, as suggested by the very small value of oxygen content (Table 1).

Anodic aluminum oxide (AAO) template-based MWCNTs is particularly suitable for the investigation into the size effect on supercapacitance due to the uniform diameter and length [69–73]. Jung et al. [70] produced AAO-based CNTs with a diameter of 50 nm and a specific surface area of 360 m^2/g using the AAO template with a diameter and length of 90 nm and 100 μm, respectively, and catalyst Co. The CNTs with the template was directly used as the electrode without removing the alumina. The specific capacitance of the template-based CNT electrodes was around 50 F/g. The enhancement of the capacitance is due to the uniformity of the template-based CNTs comparing with the non-uniform CNTs. Ahn et al. [69] found

Table 1 BET specific surface area, mesopore volume, percentage of oxygen, and capacitance of the analyzed nanotubes. ([53], Copyright @ American Institute of Physics)

Type of nanotubes	A700Co/Si	A900Co/Si	A600Co/NaY	P800/Al
*V*meso (cm^3 STP/g)	435	381	269	643
*S*BET (m^2/g)	411	396	128	311
Oxygen (mass%)	10.8	4.6	0.8	<0.3
Capacitance (F/g)	80	62	4	36

that the capacitance of the CNTs with smaller diameter (33 nm) is larger than that of with larger diameter (200 nm) due to the larger surface area in smaller diameter CNTs.

Effects of Heating

Heating is one of important ways to improve the graphitization of CNTs and remove the amorphous carbon. The effects of heating on the capacitance depend on the heating temperature and the quality of the as-grown CNTs. The capacitance of as-received SWCNTs (Rice) was about 40 F/g and reduced to 18 F/g after heating treatment at 1,650 °C probably due to the more perfect graphitization of the tubes [74]. However, Li et al. [75] found that the specific capacitance was increased by the oxidization up to 650 °C due to the enhanced specific surface area and dispersity. But the capacitance decreased with further increasing the temperature due to reduced surface area. At the same time, the heat treatment led to the reduction in the equivalent series resistance, resulting in the enhancement of the power density because of the improvement on graphitization. Fig. 2 shows the Brunauer-Emmett-Teller (BET; N_2) specific surface area and average pore diameter of as-grown CNTs as a function of heat-treatment temperature (carried out for 30 min) [54, 76]. With increasing temperature, the specific surface area increases, whereas the average pore diameter decreases and saturates at high temperature. The raw sample shows a peak at 150 Å and has less distribution in the smaller pore diameter near 20 Å. With increasing heat-treatment temperature, the number of smaller pore diameters increases and reaches the maximum at 1,000 °C, whereas the number of pore diameters ranging from 50 ± 250 Å decreases. Fig. 3 shows the specific capacitance as a function of charging time and current, the CV curves, and impedance plots. A maximum specific capacitance of 180 F/g and a measured power density of 20 kW/kg for the heat-treated SWCNTs were obtained. The increased capacitance was well explained by the enhancement of the specific surface area and the abundant pore distributions at lower pore sizes.

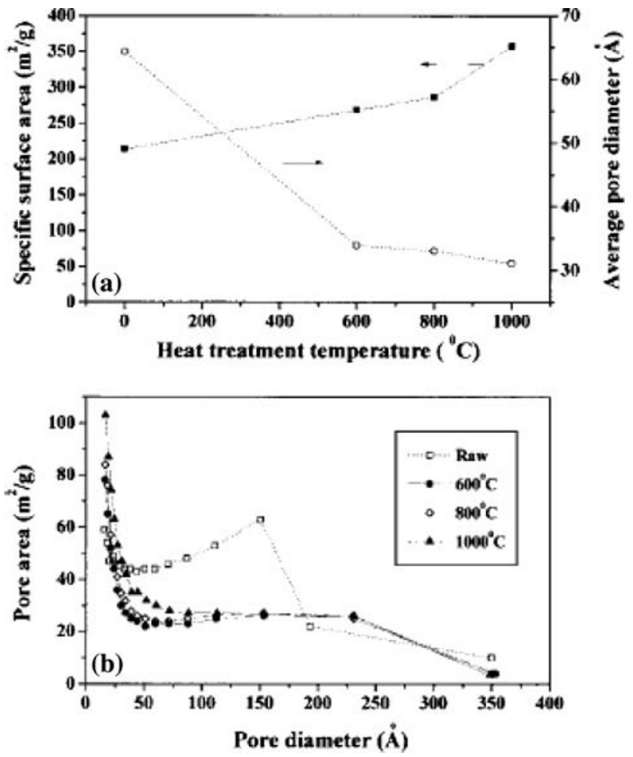

Fig. 2 (**a**) The BET (N_2) specific surface areas and the average pore diameters of the CNT electrode as a function of heat-treatment temperature and (**b**) The pore size distribution of the CNT electrodes. ([54], Copyright @ Willey-VCH)

Effects of Functionalization

Capacitance of CNT-based supercapacitor can also be enhanced by chemical activation [56, 77, 78], functionalization [79–81], and heat and surface treatment [81, 82]. The value of specific capacitance increased significantly after strong oxidation in nitride acid due to the increase of the functional groups on the CNT's surface [56]. Enhanced values of capacitance were observed after activation: in some cases, it increased almost seven times, because the microporosity of pure MWCNTs can be highly developed using chemical KOH activation [77]. The activated material still possessed a nanotubular morphology with many defects on the outer walls that gave a significant increase in micropore volume, while keeping a noticeable mesoporosity. The electrochemical treatment of CNTs provides an effective and controllable method for changing the pore size distribution (PSD) of SWCNTs [78]. In particular, a remarkable volume of the small mesopores in the 3.0–5.0 nm diameter range was increased. The SWCNTs treated for 24 h at 1.5 V have a higher specific surface area (109.4 m^2/g) and larger volume of small mesopores (0.048 cm^3/g in 3.0–5.0 nm diameter range), compared with the as-grown SWCNTs (46.8 m^2/g and 0.026 cm^3/g, respectively). The specific capacitance was increased threefold after electrochemical treatment. The electric double-layer capacitance, depending on the surface functional groups, can be dramatically changed, from a large increase to complete disappearance [79]. The introduction of surface carboxyl groups created a 3.2 times larger capacitance due to the increased hydrophilicity of MWCNTs in an aqueous electrolyte. In contrast, the introduction of alkyl groups resulted in a marked decrease in capacitance. Notably, the complete disappearance of capacitance for samples functionalized with longer alkyl groups, indicating the perfect block of proton access to the carbon nanotubes'

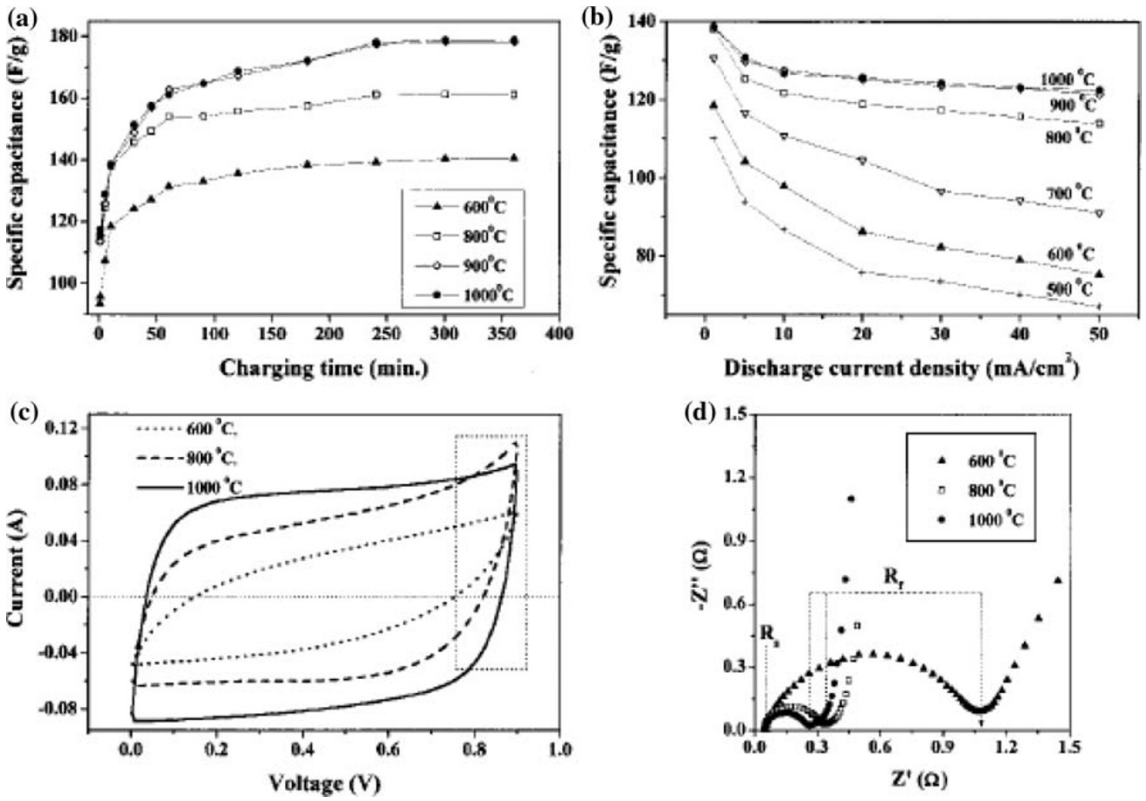

Fig. 3 Electrochemical properties of the supercapacitor using the CNT electrodes. (**a**) The specific capacitances of the heat-treated electrodes at various temperatures as a function of the charging time at a charging voltage of 0.9 V, where the capacitance was measured at a discharging current of 1 mA/cm^2. (**b**) The specific capacitances of the heat-treated electrodes at various temperatures as a function of the discharging current density at a charging voltage of 0.9 V for 10 min. (**c**) The cyclic voltammetric (*CV*) behaviors (sweep rate, 100 mV/s) for the CNT electrodes at various heat-treatment temperatures. (**d**) The complex-plane impedance plots for the CNT electrodes for various heat-treatment temperatures at an ac-voltage amplitude of 5 mV, Z″: imaginary impedance, Z′: real impedance. ([54], Copyright @ Willey-VCH)

surfaces by extreme hydrophobicity. The specific capacitance can also be enhanced by fluorine functionalization with heat treatment [80]. The fluorination of SWCNT walls transformed the nonpolar SWCNTs to the polar ones by forming dipole layers on the walls, resulting in high solubility in deionized water. Fluorinated samples gave lower capacitance than the raw samples before heat treatment due to the increase in the micropore area and the decrease in the average pore diameter. However, after heat treatment, the specific capacitance of the fluorinated samples became higher than those of the raw samples because of the additional redox reaction due to the residual oxygen gases present on the surface of the electrodes. The reduction of ERS was attributed to the improvement in conductivity because of the carrier induced by the functionalization [81]. Pyrrole treated-functionalized SWCNTs have high values of capacitance (350 F/g), power density (4.8 kW/kg), and energy density (3.3 kJ/kg) [82]. The high capacitance can also be obtained by the plasma surface treatment with NH_3 due to the enhancement of the total surface area and wettability of the MWCNTs [83].

Effects of Shape Engineering

Shape engineering of CNTs can also greatly improve the capacitance and power density [84]. When compared with activated carbon cells, the high-densely packed and aligned SWCNTs showed higher capacitance, less capacitance drop at high-power operation, and better performance for thick electrodes. Fig. 4 shows that the SWCNTs are high-densely packed after the engineering. Cyclic voltammograms of the solid sheet and forest cells were very similar, meaning the two materials have nearly the same capacitance per weight. The capacitance of the SWCNT solid EDLC was larger than that of forest cell. The energy density was estimated to be 69.4 W h/kg. Ion diffusivity plays a key factor to realize compact supercapacitors with high energy density and high power density. Because the electrolyte ions must diffuse through the pores of interstitial regions within the SWCNT packing structure, ion accessibility is limited in the inner region of the solids on the relevant timescale. Superior electrochemical properties of SWCNT solid cells originate from the aligned pore

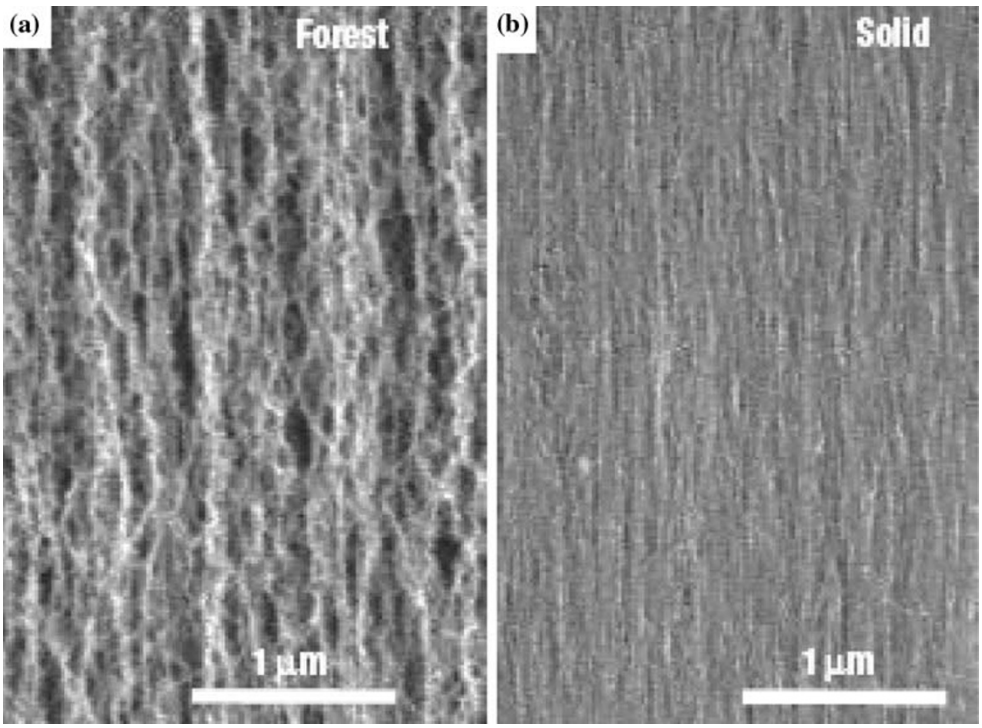

Fig. 4 SEM images of (**a**) the as-grown forest and (**b**) shape-engineered SWCNTs. ([84], Copyright @ Nature Publishing Group)

structures compared with activated carbon due to the fast and easy ion diffusivity [84].

Recently, Pan et al. [85] systematically investigated the effects of factors, such as diameter, surface area and pore size distribution, on the capacitance and demonstrated that the supercapacitance can be improved by the shape engineering. Fig. 5 shows the TEM images of AAO-based MWCNTs with a diameter of 50 nm (AM50) and AAO-based tubes-in-tube MWCANTs (ATM50). Clearly, smaller CNTs were confined with a larger one comparing (Fig. 5d–c). Fig. 6 shows the CV plots of the samples in the aqueous solution of 0.5 Mol/L H_2SO_4 at a scan rate of 50 mV/s. Two peaks on every CV plot for the five samples indicate that supercapacitors can be realized due to the existence of the Faradic processes. The Redox peaks on the CV plots can be ascribed to oxygenated groups attached to the surface of the carbon nanostructures, such as OH^- [24, 25], which leads to the remarkable pseudocapacitance. The redox reaction (faradaic process) can be considered as following [16, 25]:

$$> C - OH \Leftrightarrow C = O + H^+ + e^-$$
$$> C = O + e^- \Leftrightarrow > C - O^-.$$

The conductivity of CNTs can also be improved by the OH functionalization because of the band-gap narrowing and carrier (hole) doping [86, 87]. The better average specific capacitance of ATM50 was attributed to its higher surface area, better pore size distribution, and conductivity. The amount of electrical charge accumulated due to electrostatic attraction in EDLC depends on the area of the electrode/electrolyte interface that can be accessed by the charge carriers. The higher surface area of the electrode material could leads to higher capacitance if the area can be fully accessed by the charge carriers. However, higher surface area does not always result in higher capacitance, because the capacitance depends on the pore size and its size distribution. The surface area is hardly accessible if it consists of micropores (<2 nm) [28]. The average pore diameters of all samples are larger than 2 nm (Table 2). The pore size distributions for AM50 and ATM50 are narrow and show that the dominant pore diameter is about 3.9 nm. However, the pore size distributions for other samples are broad and extend to lager size, although the dominant pore diameter is about 2 nm for other samples (Fig. 7). The average specific capacitance for AM50 and ATM50 is larger than those of other samples. And, the average specific capacitance increases with the increase in the specific surface area with the exception of ATM50. The electrical conductivity is one of the factors that affect the capacitance. It should be mentioned that the higher the surface area, the poorer the conductivity should be. This should be one of the reasons for the capacitance of ATM50 larger than that of AM50 [85].

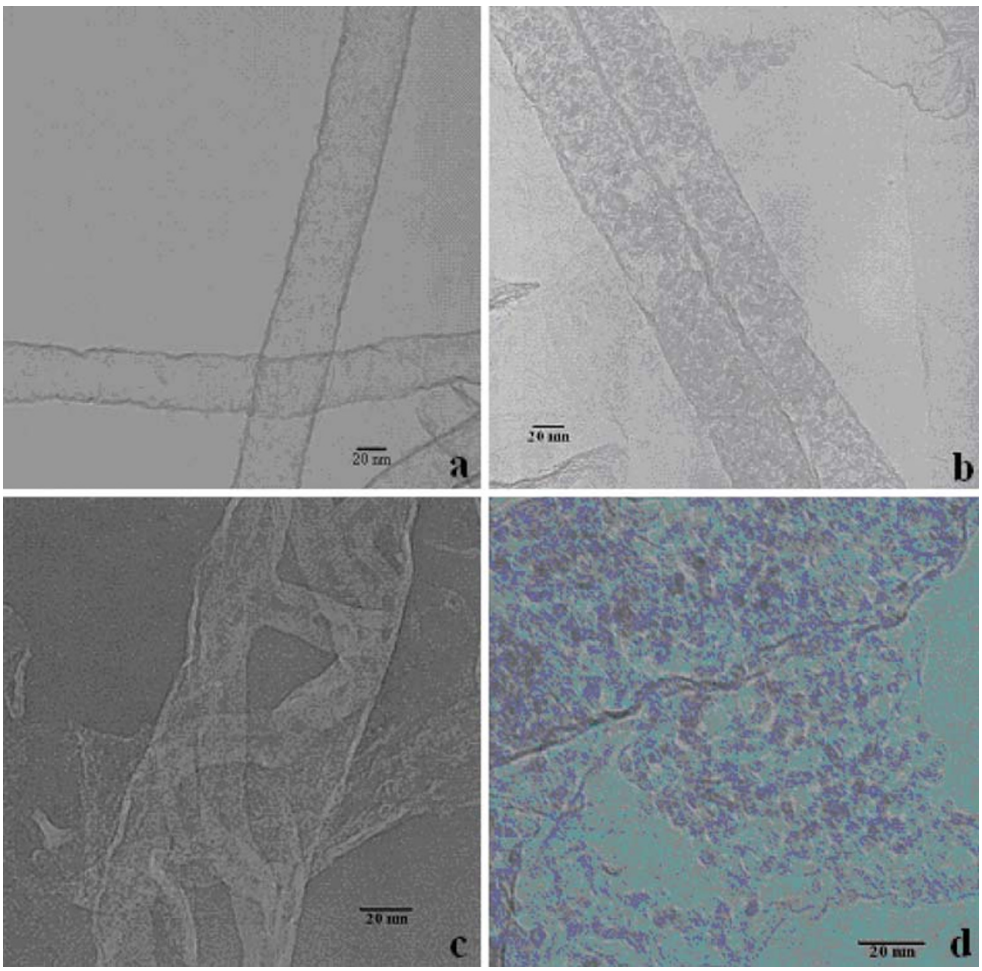

Fig. 5 TEM images of AAO-based 50 nm MWCNTs after the first- and second-step pyrolysis of C_2H_4: (**a**) AM50, (**b**) ATM50, (**c**) and (**d**) fine view of ATM50. ([85], Copyright @ American Chemical Society)

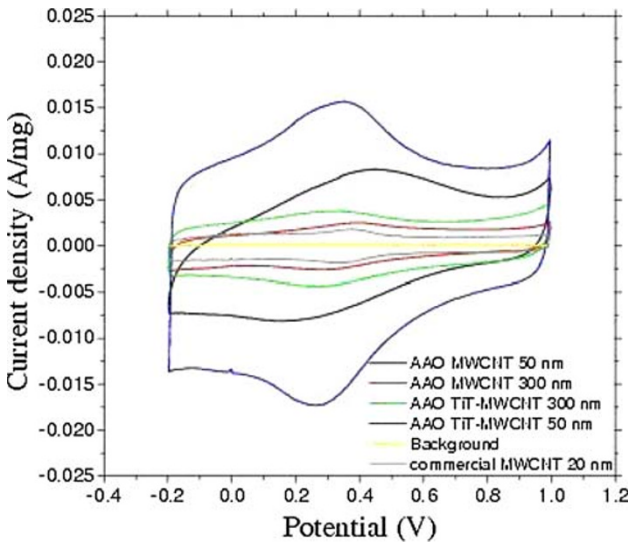

Fig. 6 The CV plots in 0.5 M H_2SO_4 at a scan rate of 50 mV/s for the five samples. ([85], Copyright @ American Chemical Society)

Table 2 Specific surface area, average pose size, and capacitance of the carbon nanomaterials. ([85], Copyright @ American chemical Society)

	CM20	AM50	AM300	ATM50	ATM300
I_D/I_G	1.03	0.86	0.92	0.74	0.84
Specific area (m^2/g)	136	649	264	500	390
Average pore diameter (nm)	8.8	3.9	7.4	5.2	9.1
Capacitance (F/g)	17	91	23	203	53

The high power density supercapacitor can also be achieved using electrophoretic deposited (EPD) CNT films and locally aligned CNTs [55, 88, 89]. The EPD film has a uniform pore structure formed by the open space between entangled nanotubes. Such an open porous structure with a high accessible surface area is unobtainable with other carbon materials and enables easy access of the solvated ions to the electrode/electrolyte interface, which is crucial

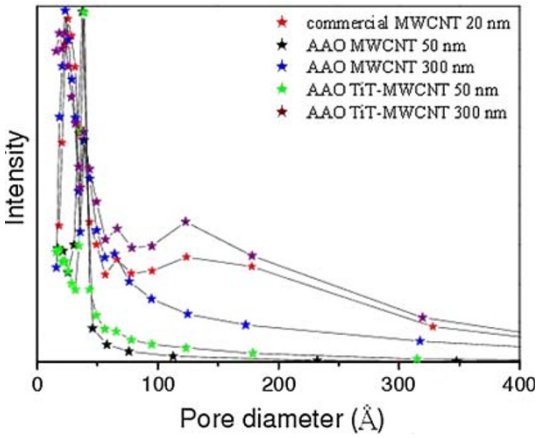

Fig. 7 The pose size distribution calculated using BJH method. ([85], Copyright @ American Chemical Society)

for charging the electric double layer. The current response profiles of the CV curves at the scan rates of 50 and 1,000 mV/s (Fig. 8) are almost ideally rectangular along the time-potential axis. The excellent CV shape reveals a very rapid current response on voltage reversal at each end potential, and the straight rectangular sides represent a very small equivalent series resistance (ESR) of the electrodes and also the fast diffusion of electrolyte in the films [1]. Fig. 9 shows the CV plots with different scan rates of the assembled supercapacitor made of high packing and aligned CNTs, which are close to an ideally rectangular shape even at exceedingly high scan rates of 500 and 1,000 mV/s, indicating an extremely low ESR of the electrodes [89]. The *E–t* responses of the charge process were almost the mirror image of their corresponding discharge counterparts, and no IR drop was observed, again owing to the negligible ESR of the electrodes. The high power density is attributed to the small internal resistance which results from the coherent structure of the thin films fabricated using a highly concentrated colloidal suspension of carbon nanotubes.

Supercapacitor from CNT and Oxide Composite

A hybrid electrode consisting of CNTs and oxide incorporates a nanotubular backbone coated by an active phase with pseudocapacitive properties, which fully utilize the advantages of the pseudocapacitance and EDLC. The open mesoporous network formed by the entanglement of nanotubes may allow the ions to diffuse easily to the active surface of the composite components and to lower the equivalent series resistance (R_s) and consequently increase the power density.

Ruthenium Oxide and CNTs Composite

Ruthenium oxide (RuO_2) has been proved to be one of important materials in oxide supercapacitors. The electrostatic charge storage as well as pseudofaradaic reactions of RuO_2 nanoparticles can be affected by the surface functionality of CNTs due to the increased hydrophilicity [90]. Such hydrophilicity enables easy access of the solvated

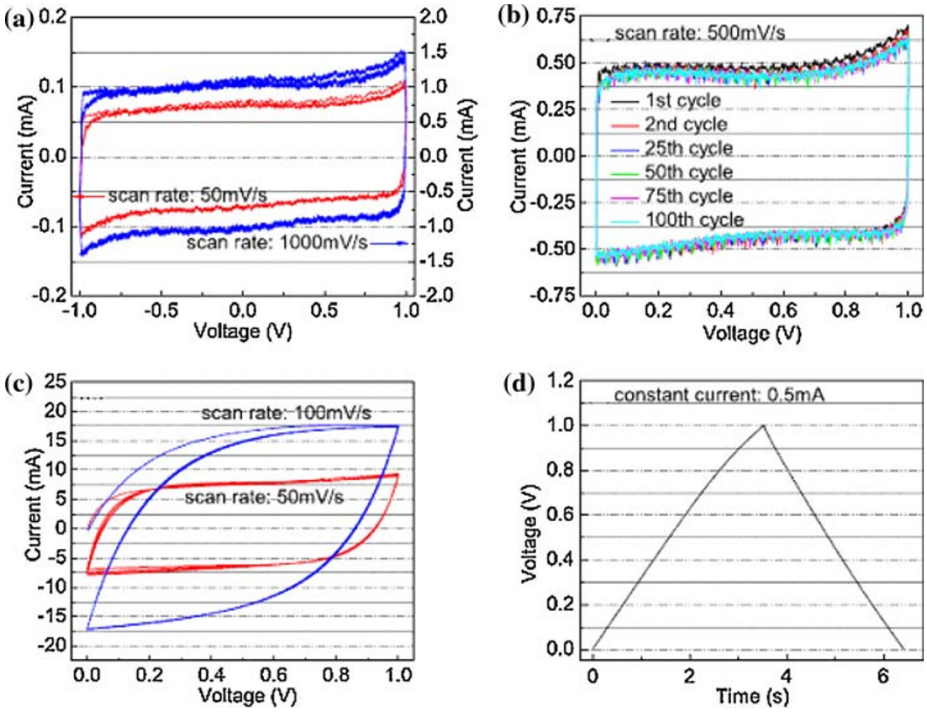

Fig. 8 (**a**) CVs of the nanotube thin film supercapacitor cycled from −1 V to +1 V, (**b**) CVs of the nanotubes thin film supercapacitor cycled from 0 V to +1 V for 100 cycles, (**c**) CVs of a conventional supercapacitor made of carbon particle thin films, and (**d**) charge/discharge curves of the nanotube thin film supercapacitor. ([55], Copyright @ Institute of Physics)

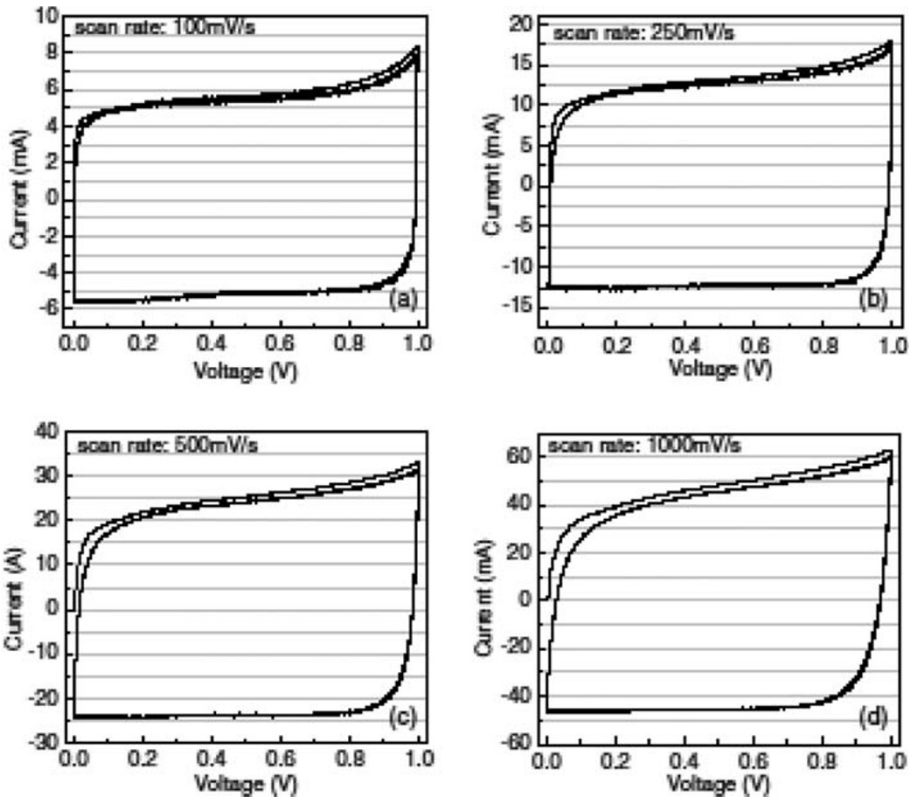

Fig. 9 Cyclic voltammograms with different scan rates of an assembled supercapacitor using the nanotube thin films as electrodes. ([89], Copyright @ Institute of Physics)

ions to the electrode/electrolyte interface, which increases faradaic reaction site number of RuO_2 nanoparticles and leads to higher capacitance. The specific capacitance of RuO_2/pristine CNT nanocomposites based on the combined mass was about 70 F/g (RuO_2: 13 wt% loading). However, the specific capacitance of RuO_2/hydrophilic CNT (nitric acid treated) nanocomposites based on the combined mass was about 120 F/g (RuO_2: 13 wt% loading). Kim et al. [91] reported that a three-dimensional CNT film substrate with RuO_2 showed both a very high specific capacitance of 1,170 F/g and a high-rate capability. To enhance its pseudocapacitance, ruthenium oxide must be formed with a hydrated amorphous and porous structure and a small size, because this structure provides a large surface area and forms conduction paths for protons to easily access even the inner part of the RuO_2. The highly dispersed RuO_2 nanoparticles can be obtained on carboxylated carbon nanotubes by preventing agglomeration among RuO_2 nanoparticles through bond formation between the RuO_2 and the surface carboxyl groups of the carbon nanotubes [92] or by treating the CNTs in a concentrated H_2SO_4/HNO_3 (3:1 volume ratio) mixture at 70 °C [93]. The highly dispersed RuO_2 nanoparticles on carbon nanotubes show an increased capacitance, because the protons are able to access the inner part of RuO_2 with the decrease in size, and its utilization is increased. The high dispersion of RuO_2 is therefore a key factor to increase the capacitance of nanocomposite electrode materials for supercapacitors. A prominently enhanced capacitive performance was also observed in well-dispersed RuO_2 nanoparticles (NPs) on nitrogen-containing carbon nanotubes [94, 95]. The function of nitrogen amalgamation is to create preferential sites on CNTs with lower interfacial energy for attachment of RuO_2 nanoparticles (Fig. 10). This crucial phenomenon leads to a

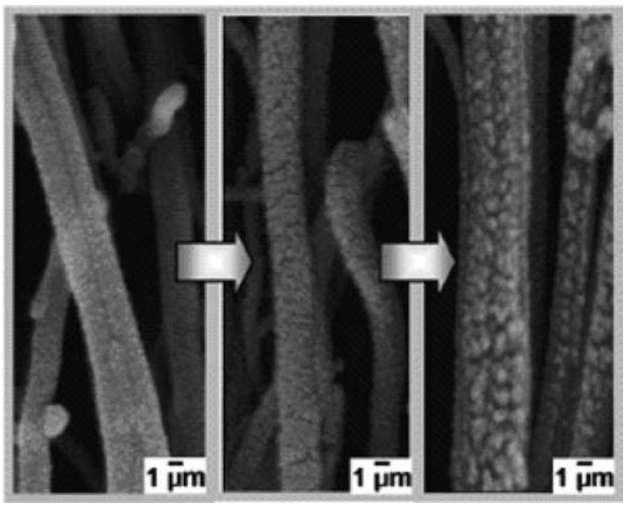

Fig. 10 Evolutionary SEM images of one single N-containing CNT capturing RuO_2 NPs under distinct coating quantity. ([94], Copyright @ American Electrochemical Society)

significant improvement in the overall specific capacitance up to the measured scan rate of 2,000 mV/s, indicating that superior electrochemical performances for supercapacitor applications can be achieved with RuO_2–CNT-based electrodes using nitrogen incorporation technique. However, the commercialization of RuO_2/CNTs composite is very difficult because of the high cost and high toxicity of RuO_2.

Co_3O_4 and CNTs composite

Co_3O_4 is also an important transition-metal oxide and has great application in heterogeneous catalysts, anode materials in Li-ion rechargeable batteries, solid-state sensors, solar energy absorbers, ceramic pigments, and electrochromic devices [96]. Shan et al. [97] reported a novel type of multi-walled carbon nanotubes (MWCNTs)/Co_3O_4 composite electrode for supercapacitors. The electrode was prepared through a facile and effective method, which combined the acid treatment of MWCNTs and in situ decomposition of $Co(NO_3)_2$ in *n*-hexanol solution at 140 °C. The MWCNTs/Co_3O_4 composites show high capacitor property, and their best specific capacitance is up to 200 F/g, which is significantly greater than that of pure MWCNTs (90 F/g).

Manganese Oxide and CNTs Composite

Manganese oxide is one of the most promising pseudocapacitor electrode materials with respect to both its specific capacitance and cost effectiveness. CNT is effective for increasing the capacitance and improving the electrochemical properties of the a-$MnO_2{\cdot}nH_2O$ electrodes and a very promising material as a conductive additive for capacitor or battery electrodes [98]. The performance of real capacitors based on manganese oxide is limited by the two irreversible reactions Mn(IV)–Mn(II) and Mn(IV)–Mn(VII), which potentially depend on the electrolyte pH. In particular, with real capacitors, the electrolyte usually leads to the dissolution of the negative electrode. The CNTs can help in preserving the electrodes integrity during cycling. The long cycle performance at a high charge–discharge current of 2 A/g for the a-MnO_2/SWCNTs composites was obtained [99]. All the composites with different SWCNT loads showed excellent cycling capability, even at the high current of 2 A/g, with the MnO_2 and 20 wt% SWCNT composite showing the best combination of efficiency of 75% and specific capacitance of 110 F/g after 750 cycles. The initial specific capacitance of the MnO_2/CNTs nanocomposite (CNTs coated with uniform birnessite-type MnO_2) in an organic electrolyte at a large current density of 1 A/g was 250 F/g, indicating excellent electrochemical utilization of the MnO_2 because the addition of CNTs as a conducting agent improved the high-rate capability of the nanocomposite considerably [100]. An in situ coating technique was used to prepare the MnO_2/MWCNT composite, where the nanosized ε-MnO_2 uniform layer (6.2 nm in thickness) covered the surface of the MWCNT and the original structure of the pristine MWCNT was retained during the coating process. The specific capacitance of the composite electrode reached 250.5 F/g, which was significantly higher than that of a pure MWCNT electrode [101].

$Ni(OH)_2$ and CNT composite

$Ni(OH)_2$ is often used in the hybrid supercapacitor with carbon (using KOH solution as electrolyte). The positive electrode materials ($Ni(OH)_2$) converts to NiOOH with the formation of proton and electron during the charge process. The rate capability of $Ni(OH)_2$ is associated with the proton diffusion in $Ni(OH)_2$ framework. The $Ni(OH)_2$/CNTs composite provided a shorter diffusion path for proton diffusion and larger reaction surface areas, as well as reduces the electrode resistance due to the high electronic conductivity of CNTs [102]. Wang et al. [102] reported that the CNTs can reduce the aggregation of $Ni(OH)_2$ nanoparticles, inducing a good distribution of the nanosized $Ni(OH)_2$ particles on the cross-linked, netlike structure CNTs. The rate capability and utilization of $Ni(OH)_2$ were greatly improved, and the composite electrode resistance was reduced. A specific energy density of 32 Wh/kg at a specific power density of 1,500 W/kg was obtained in the hybrid supercapacitor. The capacitance can be further improved by heating the $Ni(OH)_2$/CNTs composite at 300 °C because of the formation of an extremely NiO_x thin layer on CNT film [103]. The specific capacitance decreased with the increase in NiO_x in the composite if the NiO_x percentage was above 8.9 wt%. A specific capacitance of 1,701 F/g was reported for 8.9 wt% NiO_x/CNT electrode.

Other Oxides and CNTs Composites

The Ni–Co oxides/CNT composite electrode, prepared by adding and thermally decomposing nickel and cobalt nitrates directly onto the surface of carbon nanotube/graphite electrode, has excellent charge–discharge cycle stability (0.2% loss of the specific capacitance at the 1,000th charge–discharge cycles) and good charge–discharge properties at high current density [104]. The specific capacitance of the composite increases significantly with a decrease in Ni/Co molar ratio when cobalt content is below 50% (in molar ratio) and then decreases rapidly when cobalt content is in the range between 50 and 100%.

A maximum value of the specific capacitance (569 F/g) was obtained at Ni/Co molar ratio = 1:1. Also, the specific capacitance of the nickel–cobalt oxides/CNT (Ni/Co = 1:1) electrode is much larger than the simple sum of the specific capacitances of the nickel oxide/CNT and cobalt oxide/CNT electrodes. Su et al. [105] reported a self-hybrid composite electrode composing of MWCNT and Co–Al-layered double hydroxides. The CV curves approached rectangle shapes, and the charge and discharge curves were basically symmetrical. Compared to MWCNTs supercapacitor, this new supercapacitor has good long-term stability, larger maximum power (6,400 W/kg) and energy density (13.2 Wh/kg), and a higher specific capacitance of 15.2 F/g even after 1,000 cycles at a large current of 2 A/g.

The capacitance of V_2O_5/CNTs composite is also larger than those of pure V_2O_5 and CNTs [106]. The addition of SnO_2 to the V_2O_5/CNTs can further increase the capacitance, because SnO_2 can improve the electronic properties of V_2O_5. The $LiNi_{0.8}Co_{0.2}O_2$/MWCNT (5–15 nm in diameter) composite capacitor has a specific capacitance and energy density of 270 F/g and 317 Wh/kg, respectively [107]. The MWCNTs substantially improves the electrochemical performance of the $LiNi_{0.8}Co_{0.2}O_2$-based capacitor because of the combination of increased conductivity, proper pore distributions, good mechanical properties, and electrolyte accessibility. A chromium oxide/SWCNT-based electrodes shows exceptionally quick charge propagation due to the overall physical and textural properties of SWCNT [60]. Nanosized chromium oxide particles finely dispersed at nanoscale in the SWCNT make possible the enhanced charging rate of the electrical double layer and allow fast faradaic reactions. Chromium-containing species present as CrO_3 inside SWCNTs as well as in the form of CrO_2Cl_2 (possibly along with CrO_3 too) between SWCNTs within bundles supply redox reactions due to access by the electrolyte in spite of its encapsulated (and intercalated) location because of the numerous side openings created all along the SWCNT defective walls during the filling step.

Reddy et al. [108] compared the electrochemical properties of RuO_2/MWCNT, TiO_2/MWCNT, and SnO_2/MWCNT nanocrystalline composites for supercapacitor electrodes. The average specific capacitances measured using the three electrochemical techniques of the pure MWCNT, RuO_2/MWCNT, TiO_2/MWCNT, and SnO_2/MWCNT nanocomposite electrodes are 67, 138, 160, and 93 F/g, respectively. The enhancement of the specific capacitance of metal oxide dispersed MWCNT from pure MWCNT is due to the progressive redox reactions occurring at the surface and bulk of transition metal oxides through faradaic charge transfer due to the modification of the surface morphology of MWCNT by the nanocrystalline RuO_2, TiO_2, and SnO_2.

Supercapacitor from CNT and Polymer Composite

Electronically conducting polymers are promising supercapacitor materials for two main reasons: (1) high specific capacitance because the charge process involves the entire mass and (2) high conductivity in charged state, leading to low ESR and high power density. The main drawback using polymer in supercapacitor is the cycling stability because of typical shrinkage, breaking, and cracks appearing in subsequent cycles. It has been already proved that composites based on CNTs and conducting polymers, such as polypyrrole and polyaniline, are very interesting electrode materials, because the entangled mesoporous network of nanotubes in the composite can adapt to the volume change. That allows the shrinkage to be avoided, and hence a more stable capacitance with cycling to be obtained.

Polymer and CNTs Hybrid Composite

Lota et al. [3] reported a novel composite material prepared from a homogenous mixture of polymer poly(3,4-ethylenedioxythiophene; PEDOT) and CNTs or by chemical or electrochemical polymerization of EDOT directly on CNTs. The optimal proportions of the composite are 20–30% of CNTs and 70–80% of PEDOT. Among the three methods used for the composites preparation, the electrochemical method gave the best capacitance results (150 F/g). And such material had a good cycling performance with a high stability in all the electrolytes. Another quite important advantage of this composite is its significant volumetric energy because of the high density of PEDOT. Due to the open mesoporous network of nanotubes, the easily accessible electrode/electrolyte interface allows quick charge propagation in the composite material and an efficient reversible storage of energy in PEDOT during subsequent charging/discharging cycles.

The capacitance values for the composites [20 wt% of CNTs and 80 wt% of conducting polymers (ECP), such as polyaniline (PANI) and polypyrrole (PPy)] strongly depend on the cell construction [109]. In the case of three electrode cells, extremely high values could be found from 250 to 1100 F/g; however, in the two-electrode cell, much smaller specific capacitance values of 190 F/g for PPy/CNTs and 360 F/g for PANI/CNTs had been measured. It highlights the fact that only two-electrode cells allow a good estimation of materials performance in electrochemical capacitors. The CNTs/PPy film shows excellent charge storage and transfer capabilities, attributed to the high surface area, conductivity, and electrolyte accessibility of the nanoporous structure [64]. The aligned CNTs/PPy composite film had an exciting combination of exceptional charge storage capacities as large as 2.25 F/cm^2 and

improved device response times relative to pure PPy films. The superior performance of the composite relative to their component materials is attributed to the combination of electrolyte accessibility, reduced diffusion distances, and improved conductivity in the redox-pseudocapacitive composite structure. An et al. [110] demonstrated that the SWCNT/PPy (1/1 in weight) nanocomposite electrode shows much higher specific capacitance than pure PPy and as-grown SWCNT electrodes, due to the uniformly coated PPy on the SWNTs. A maximum specific capacitance of 265 F/g from the SWNTs/PPy nanocomposite electrode containing 15 wt% of the conducting agent was obtained. The addition of conducting agent into the SWCNT-PPy nanocomposite electrode gives rise to an increase in the specific capacitance by reducing the internal resistance of the supercapacitor.

The specific capacitance of PANI/SWCNT composite electrode increased as the amount of the deposited PANI onto SWCNTs increases up to 73 wt%, where the PANI was wrapped around SWCNT [111]. Beyond 73 wt%, the additional PANI was deposited either in the mesopores between SWCNTs or in the form of film over the surface, which caused drop in the capacitance. The trend of the capacitance as a function of the PANI weight was opposite to that of specific resistivity. The highest specific capacitance, specific power, and specific energy values of 485 F/g, 228Wh/kg and 2,250 W/kg were observed for 73 wt% PANI deposited onto SWCNTs. And the PANI/SWCNT composites showed long cyclic stability. Figure 11 shows the specific capacitance of PANI/SWCNT composite films electrodes as a function of discharge current density [112]. The SWCNT/PANI composite film shows a higher specific capacitance, because the presence of SWCNT in the growth solution could promote the rate of aniline polymerization and result in a smooth, uniform, and highly porous composite film with a higher doping degree and lower defect density compared to the rough spherical grain-based pure PANI film. A MWCNT/PANI composite synthesized by an in situ chemical oxidative polymerization method showed much higher specific capacitance (328 F/g) because MWCNT made the composites had more active sites for faradiac reaction [113]. Similarly, the highest specific capacitance value of 224 F/g was obtained for the MWCNT/PANI composite materials containing MWCNTs of 0.8 wt% [114]. The same composite (MWCNT/PANI) synthesized by microwave-assisted polymerization was a core–shell structure with PANI layers (50–70 nm), which has an enhanced specific capacitance of 322 F/g with a specific energy density of 22 W h/kg [115].

The CNTs/PAN composite with a ratio of 30/70 between CNT and PAN pyrolysized from a CNT/PAN blends for 180 min gave a high capacitance (100 F/g) although its specific surface area (157 m^2/g) is not the highest compared with the 50/50 CNT/PAN composite (233 m^2/g, 57 F/g) [116]. This suggested that the content of PAN must be high enough not only to favor a large gas evolution, which develops porosity, but also to obtain the highest amount of residual nitrogen in the negative and positive ranges of potential, respectively, which contributed more to the pseudofaradiac charge transfer reactions.

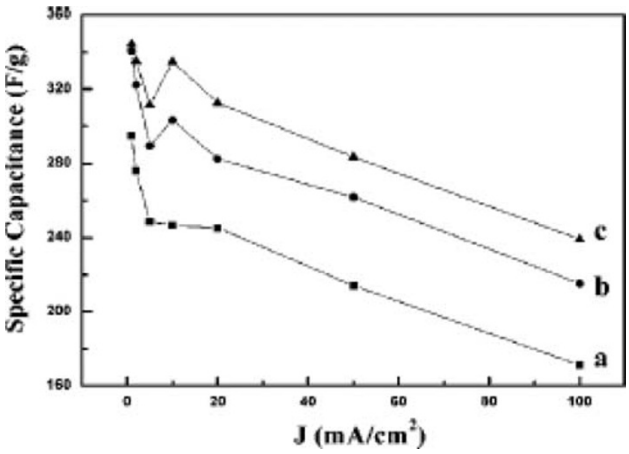

Fig. 11 Specific capacitances of the SWNT/PANI composite film prepared from the growth solutions with (**a**) 0, (**b**) 4, and (**c**) 8 wt% SWCNT as a function of current density. ([112], Copyright @ American Electrochemical Society)

Polymer and CNTs Ternary Composites

Single wall carbon nanotubes in the ternary composite, PAN/SAN/SWCNTs, acted as a compatabilizer for polyacrylonitrile (PAN)/styreneeacrylonitrile (SAN) copolymer blends, which was used to develop porosity control in the carbonized PAN/SAN/SWCNT composites with an average pore size in the range of 3–13 nm [117]. Extremely high electrical double-layer capacity in the range of 83–205 mF/cm^2 was observed in the ternary composites.

DNA and CNTs Composite

DNA is a good candidate for improved electrical conductivity for electrochemical devices with CNTs, because DNA has electrical characteristics similar to those of semiconducting diodes. In addition, DNA can more effectively coat, separate, and solubilize CNTs than other surfactants because of the large surface area of its phosphate backbone, which interacts with water, and there are many bases in DNA that can bind to CNTs. Therefore, DNA wrapping can debundle CNTs in high concentration

CNT dispersions. Recently, Shin et al. [118] reported the DNA-wrapped SWCNT hydrid fibers for supercapacitor electrode materials. The DNA–SWNT hybrid fibers were obtained using the wet-spinning method reported previously. The capacitance of the DNA-wrapped SWCNT fibers was 60 F/g (in a phosphate buffered saline solution), larger than that of pure SWCNT mat (30 F/g) due to the improved electrical conductivity, high CNT surface area and enhanced mechanical stability due to the π–π interaction between the DNA and the CNT sidewall.

Summary

Supercapacitor, as an energy storage device, have been studied and used in many fields. The electrode material of the supercapacitor needs to satisfy three basic requirements: (1) high capacitance, (2) low resistance, and (3) stability. CNT-based electrode materials, including CNTs, CNT/oxide composite, and CNT/polymer composite, have been widely studied in past decade and attracting increasing attentions for their application to supercapacitor due to their satisfaction to the criteria.

As the electric-double-layer capacitor, the performance of the CNT-based supercapacitor is closely related to the physical properties of the CNTs, such as specific surface area. The performance should depend on the synthesis and post-treatment methods of the CNTs. It is clear that the specific surface area is not the solely dominant factor to the performance. The capacitance of the CNTs is affected by various factors, including specific surface area, pore size, pore size distribution, conductivity, etc. Only by optimizing these factors can the performance be improved. Various methods have been proposed for the purpose, such as functionalization, oxidization, and doping, which can lead to high capacitance through the improvement in conductivity, fast ion diffusivity, and addition of pseudocapacitance. Other methods were introduced to modify the structure of the CNTs, such as densely packed and ordered CNTs and tubes-in-tube CNTs, which result in the improvement in the capacitance and conductivity without introducing any functional groups. High stability should be achieved by these modifications. Although the capacitance of the pure CNTs was enhanced and its stability was improved, the capacitance of CNT-based supercapacitor is still lower than that of amorphous carbon or porous carbon and can be enhanced by optimizing the surface area, pore size, and pore size distribution.

High capacitance can also be achieved by using the mixture of the CNTs with oxide, polymer, or both as the electrode. The hybrid supercapacitor requires that the oxide nanoparticles should be chemically attached to the walls of CNTs or the CNTs should be uniformly covered by the polymer with accurately controlled thickness. And the ratio between the oxide/polymer and CNTs is critical to the enhancement of the capacitance. Presently, there has no general answer to the ratio in literatures because the starting materials, CNTs, oxide, and polymer, and processing methods are different from literature to literature. The systematical investigations are needed to solve this problem. However, the stability of the hybrid supercapacitor is still questionable.

References

1. B.E. Conway, *Electrochemical Supercapacitors: Scientific Fundamentals And Technological Applications* (Kluwer Academic/Plenum, New York, 1999)
2. Website: http://en.wikipedia.org/wiki/Supercapacitor
3. K. Lota, V. Khomenko, E.J. Frackowiak, J. Phys. Chem. Solids **65**, 295 (2004)
4. S.K. Ryu, X. Wu, Y.G. Lee, S.H. Chang, J. Appl. Polym. Sci. **89**, 1300 (2003)
5. S. Patra, N. Munichandraiah, J. Appl. Polymer Sci. **106**, 1160 (2007)
6. F. Marchioni, J. Yang, W. Walker, F. Wudl, J. Phys. Chem. B **110**, 22202 (2006)
7. K.S. Ryu, Y.G. Lee, Y.S. Hong, Y.J. Park, X.L. Wu, K.M. Kim, M.G. Kang, N.G. Park, S.H. Chang, Electrochim. Acta **50**, 843 (2004)
8. M.D. Ingram, H. Staesche, K.S. Ryder, Solid State Ionics **169**, 51 (2004)
9. K.R. Prasad, N. Munichandraiah, Electrochem. Solid State Lett. **5**, A271 (2002)
10. J.Y. Kim, I.J. Chung, J. Electrochem. Soc. **140**, A1376 (2002)
11. K.S. Ryu, K.M. Kim, N.G. Park, Y.J. Park, S.H. Chang, J. Power Sources **103**, 305 (2002)
12. J.C. Lassegues, J. Grondin, T. Becker, L. Servant, M. Hernandez, Solid State Ionics **77**, 311 (1995)
13. K.H. Chang, C.C. Hu, Electrochem. Solid State Lett. **7**, A466 (2004)
14. D. Rochefort, D. Guay, Alloys Compd. **400**, 257 (2005)
15. J.N. Broughton, M.J. Brett, Electrochim. Acta **49**, 4439 (2005)
16. P. Ragupathy, H.N. Vasan, N. Munichandraiah, J. Power Sources **155**, A34 (2008)
17. K. Macounová, I. Jirka, A. Trojánek, M. Makarova, Z. Samec, P. Krtil, J. Electrochem. Soc. **154**, A1077 (2007)
18. M.W. Xu, D.D. Zhao, S.J. Bao, H.L. Li, J. Solid State Electrochem. **11**, 1101 (2007)
19. T.P. Gujar, V.R. Shinde, C.D. Lokhande, W.Y. Kim, K.D. Jung, O.S. Joo, Electrochem. Communica. **9**, 504 (2007)
20. S.L. Kuo, J.F. Lee, N.L. Wu, J. Electrochem. Soc. **154**, A34 (2007)
21. K. Yokoshima, T. Shibutani, M. Hirota, W. Sugimoto, Y. Murakami, Y. Takasu, J. Power Sources **160**, 1480 (2006)
22. A. Jayalakshmi, N. Venugopal, K.P. Raja, M.M. Rao, J. Power Sources **158**, 1538 (2006)
23. S.H. Lee, C.E. Tracy, J.R. Pitts, Electrochem. Solid State Lett. **7**, A299 (2004)

24. Y.B. Mo, M.R. Antonio, D.A. Scherson, J. Phys. Chem. B **104**, 9777 (2000)
25. J.M. Miller, B. Dunn, T.D. Tran, R.W. Pekala, J. Electrochem. Soc. **144**, L309 (1997)
26. B.E. Conway, J. Electrochem. Soc. **138**, 1539 (1991)
27. J.H. Jiang, A. Kucernak, Electrochim. Acta **47**, 2381 (2002)
28. L.M. Huang, H.Z. Lin, T.C. Wen, A. Gopalan, Electrochim. Acta **52**, 1058 (2006)
29. J.W. Long, K.E. Swider, C.I. Merzbacher, D.R. Rolison, Langmuir **15**, 780 (1999)
30. H.I. Becker, Low voltage electrolytic capacitor, US patent 2800616
31. E. Frackowiak, F. Beguin, Carbon **39**, 937 (2001)
32. E. Frackowiak, Phys. Chem. Chem. Phys. **9**, 1774 (2007)
33. J. Chmiola, G. Yushin, Y. Gogotsi, C. Portet, P. Simon, P.L. Taberna, Science **313**, 1760 (2006)
34. E. Raymundo-Piñero, F. Leroux, F. Béguin, Adv. Mater. **18**, 1877 (2006)
35. A.B. Fuertes, G. Lota, T.A. Centeno, E. Frackowiak, Electrochim. Acta **50**, 2799 (2005)
36. D. Hulicova, J. Yamashita, Y. Soneda, H. Hatori, M. Kodama, Chem. Mater. **17**, 1241 (2005)
37. K. Leitner, A. Lerf, M. Winter, J.O. Besenhard, S. Villar-Rodil, F. Suarez-Garci, A. Martinez-Alonso, J.M.D. Tascon, J. Power Sources **153**, 419 (2000)
38. P.J. Mahon, G.L. Paul, S.M. Keshishian, A.M. Vassallo, J. Power Sources **91**, 68 (2000)
39. N.L. Wu, S.Y. Wang, J. Power Sources **110**, 233 (2002)
40. C. Portet, P.L. Taberna, P. Simon, C. Laberty-Robert, Electrochim. Acta **49**, 205 (2004)
41. C. Kim, K.S. Yang, Appl. Phys. Lett. **83**, 1216 (2003)
42. C. Vix-Guterl, S. Saadallah, K. Jurewicz, E. Frackowiak, M. Reda, J. Parmentier, J. Patarin, F. Beguin, Mater. Sci. Engineer. B **108**, 148 (2004)
43. D. Kalpana, K.S. Omkumar, S.S. Kumar, N.G. Renganathan, Electrochim. Acta **52**, 2309 (2006)
44. M. Min, K. Machida, J.H. Jang, K. Naoi, J. Electrochem. Soc. **153**, A334 (2006)
45. C. Arbizzani, M. Mastragostino, L. Meneghello, R. Paraventi, Adv. Mater. **8**, 331 (1996)
46. J.M. Miller, B. Dunn, Langmuir **15**, 799 (1999)
47. S. Iijima, Nature **354**, 56 (1991)
48. M.S. Dresselhaus, G. Dresselhaus, P.C. Eklund, *Science of Fullerenes and Carbon Nanotubes* (Academic, New York/San Diego, 1996)
49. R. Saito, G. Dresselhaus, M.S. Dresselhaus, J. Appl. Phys. **73**, 494 (1993)
50. M.S. Dresselhaus, G. Dresselhaus, R. Saito, Solid State Commun. **84**, 201 (1992)
51. J.P. Issi, L. Langer, J. Heremans, C.H. Olk, Carbon **33**, 941 (1995)
52. T.W. Ebbesen, H.J. Lezec, H. Hiura, J.W. Bennett, H.F. Ghaemi, T. Thio, Nature **382**, 54 (1996)
53. C. Niu, E.K. Sichel, R. Hoch, D. Moy, H. Tennent, Appl. Phys. Lett. **70**, 1480 (1997)
54. K.H. An, W.S. Kim, Y.S. Park, Y.C. Choi, S.M. Lee, D.C. Chung, D.J. Bae, S.C. Lim, Adv. Mater. **13**, 497 (2001)
55. C.S. Du, N. Pan, Nanotechnol. **17**, 5314 (2006)
56. E. Frackowiak, K. Metenier, V. Bertagna, F. Beguin, Appl. Phys. Lett. **77**, 2421 (2000)
57. A.L.M. Reddy, F.E. Amitha, I. Jafri, S. Ramaprabhu, Nanoscale Res. Letts. **3**, 145 (2008)
58. C.G. Liu, M. Liu, F. Li, H.M. Cheng, Appl. Phys. Let. **92**, 143108 (2008)
59. J.N. Barisci, G.G. Wallace, D. Chattopadhyay, F. Papadimitrakopoulos, R.H. Baughman, J. Electrochem. Soc. **150**, E409 (2003)
60. L.H. Su, X.G. Zhang, C.Z. Yuan, B. Gao, J. Electrochem. Soc. **155**, A110 (2008)
61. C.Y. Lee, H.M. Tsai, H.J. Chuang, S.Y. Li, P. Lin, T.Y. Tseng, J. Electrochem. Soc. **152**, A716 (2005)
62. G. Arabale, D. Wagh, M. Kulkarni, I.S. Mulla, S.P. Vernekar, K. Vijayamohanan, A.M. Rao, Chem. Phys. Lett. **376**, 207 (2003)
63. K. Liang, K. An, Y. Lee, J. Mater. Sci. Eng. **21**, 292 (2005)
64. M. Hughes, G.Z. Chen, M.S.P. Shaffer, D.J. Fray, A.H. Windle, Chem. Mater. **14**, 1610 (2002)
65. J.N. Barisci, G.G. Wallace, R.H. Baughman, J. Electrochem. Soc. **147**, 4580 (2000)
66. S. Shiraishi, H. Kurihara, K. Okabe, D. Hulicova, A. Oya, Electrochem. Commun. **4**, 593 (2002)
67. H. Zhang, G.P. Cao, Y.S. Yang, Nanotechnol. **18**, 195607 (2007)
68. H. Zhang, G.P. Cao, Y.S. Yang, Z.N. Gu, J. Electrochem. Soc. **155**, K19 (2008)
69. H.J. Ahn, J.I. Sohn, Y.S. Kim, H.S. Shim, W.B. Kim, T.Y. Seong, Electrochem. Commun. **8**, 513 (2006)
70. M. Jung, H.G. Kim, K. Lee, O.S. Joo, S.I. Mho, Electrochim. Acta **50**, 857 (2004)
71. G. Che, B.B. Lakshmi, E.R. Fisher, C.R. Martin, Nature **393**, 346 (1998)
72. H. Pan, J.Y. Lin, Y.P. Feng, H. Gao, IEEE Trans. Nanotechnol. **3**, 462 (2004)
73. H. Pan, H. Gao, S.H. Lim, Y.P. Feng, J. Lin, J. Nanosci. Nanotech. **4**, 1014 (2004)
74. E. Frackowiak, K. Jurewicz, S. Delpeux, F. Beguin, J. Power Sources **822**, 97–98 (2001)
75. C. Li, D. Wang, T. Liang, X. Wang, J. Wu, X. Hu, J. Liang, Powder Technol. **142**, 175 (2004)
76. K.H. An, W.S. Kim, Y.S. Park, J.M. Moon, D.J. Bae, S.C. Lim, Y.S. Lee, Y.H. Lee, Adv. Funct. Mater. **11**, 387 (2001)
77. E. Frackowiak, S. Delpeux, K. Jurewicz, K. Szostak, D. Cazorla-Amoros, F. Beguin, Chem. Phys. Lett. **261**, 35 (2002)
78. C.G. Liu, H.T. Fang, F. Li, M. Liu, H.M. Cheng, J. Power Sources **160**, 758 (2006)
79. Y.T. Kim, Y. Ito, K. Tadai, T. Mitani, U.S. Kim, H.S. Kim, B.W. Cho, Appl. Phys. Lett. **87**, 234106 (2005)
80. J.Y. Lee, K.H. An, J.K. Heo, Y.H. Lee, J. Phys. Chem. B **107**, 8812 (2003)
81. H. Pan, Y.P. Feng, J. Lin, J. Phys, Conden. Matter **18**, 5175 (2006)
82. C. Zhou, S. Kumar, C.D. Doyle, J.M. Tour, Chem. Mater. **17**, 1997 (2005)
83. B.J. Yoon, S.H. Jeong, K.H. Lee, H.S. Kim, C.G. Park, J.H. Han, Chem. Phys. Lett. **380**, 170 (2004)
84. D.N. Futaba, K. Hata, T. Yamada, T. Hiraoka, Y. Hayamizu, Y. Kakudate, O. Tanaike, H. Hatori, M. Yumura, S. Iijima, Nature Mater. **5**, 987 (2006)
85. H. Pan, C.K. Poh, Y.P. Feng, J. Lin, Chem. Mater. **19**, 6120 (2007)
86. H. Pan, Y.P. Feng, J. Lin, Phys. Rev. B **70**, 245425 (2004)
87. H. Pan, Y.P. Feng, J. Lin, J. Comput. Theor. Nanosci. **5**, 2233 (2008)
88. C.S. Du, N. Pan, J. Power Sources **160**, 1487 (2006)
89. C.S. Du, J. Yeh, N. Pan, Nanotechnol. **16**, 350 (2005)
90. J.H. Park, J.M. Ko, O.O. Parka, J. Electrochem. Soc. **150**, A864 (2003)
91. H. Kim, J.H. Kim, K.B. Kim, Electrochem. Solid-State Lett. **8**, A369 (2005)

92. Y.T. Kim, K. Tadai, T. Mitani, J. Mater. Chem. **15**, 4914 (2005)
93. Y.T. Kim, T. Mitani, Appl. Phys. Lett. **89**, 033107 (2006)
94. W.C. Fang, M.S. Leu, K.H. Chen, L.C. Chen, J. Electrochem. Soc. **155**, K15 (2008)
95. W.C. Fang, K.H. Chen, L.C. Chen, Nanotechnol. **18**, 485716 (2007)
96. K. Ramachandram, C.O. Oriakhi, M.M. Lerner, V.R. Koch, Mater. Res. Bull. **31**, 767 (1996)
97. Y. Shan, L. Gao, Mater. Chem. Phys. **103**, 206 (2007)
98. E. Raymundo-Pinero, V. Khomenko, E. Frackowiak, F. Beguin, J. Electrochem. Soc. **152**, A229 (2005)
99. V. Subramanian, H. Zhu, B. Wei, Electrochem. Commun. **8**, 827 (2006)
100. S.B. Ma, K.W. Nam, W.S. Yoon, X.Q. Yang, K.Y. Ahn, K.H. Oh, K.B. Kim, J. Power Sources **178**, 483 (2008)
101. X. Xie, L. Gao, Carbon **45**, 2365 (2007)
102. Y.G. Wang, L. Yu, Y.Y. Xia, J. Electrochem. Soc. **153**, A743 (2006)
103. K. Nam, K. Kim, E. Lee, W. Yoon, X. Yang, K. Kim, J. Power Sources **182**, 642 (2008)
104. Z. Fan, J. Chen, K. Cui, F. Sun, Y. Xu, Y. Kuang, Electrochim. Acta **52**, 2959 (2007)
105. M. Jayalakshm, M.M. Raoa, N. Venugopal, K.B. Kim, J. Power Sources **166**, 578 (2007)
106. G. Wang, M. Qu, Z. Yu, R. Yuan, Mater. Chem. Phys. **105**, 169 (2007)
107. G. Lota, E. Elzbieta Frackowiak, J. Mittal, M. Monthioux, Chem. Phys. Lett. **434**, 73 (2007)
108. A.L.M. Reddy, S. Ramaprabhu, J. Phys. Chem. C Nanomater. Interfaces **111**, 7727 (2007)
109. V. Khomenko, E. Frackowiak, F. Beguin, Electrochim. Acta **50**, 2499 (2005)
110. K.H. An, K.K. Jeon, J.K. Heo, S.C. Lim, D.J. Bae, Y.H. Lee, J. Electrochem. Soc. **149**, A1058 (2002)
111. V. Gupta, N. Miura, Electrochim. Acta **52**, 1721 (2006)
112. Y.K. Zhou, B.L. He, W.J. Zhou, H.L. Li, J. Electrochem. Soc. **151**, A1052 (2004)
113. B. Dong, B.L. He, C.L. Xu, H.L. Li, Mater. Sci. Eng. B **143**, 7 (2007)
114. L.B. Kong, J. Zhang, J.J. An, Y.C. Luo, L. Kang, J. Mater. Sci. **43**, 3664 (2008)
115. H. Mi, X. Zhang, S. An, X. Ye, S. Yang, Electrochem. Commun. **9**, 2859 (2007)
116. F. Beguin, K. Szostak, G. Lota, E. Frackowiak, Adv. Mater. **7**, 2380 (2005)
117. C. Zhou, T. Liu, T. Wang, S. Kumar, Electrochim. Acta **52**, 1721 (2006)
118. S.R. Shin, C.K. Lee, I. So, J.H. Jeon, T.M. Kang, C. Kee, S.I. Kim, G.M. Spinks, G.G. Wallace, S.J. Kim, Adv. Mater. **20**, 466 (2008)